The Development of the Next Generation BSIM for Sub-100nm Mixed-Signal Circuit Simulation

Xuemei (Jane) Xi, Jin He, Mohan Dunga, Chung-Hsun Lin, Babak Heydari, Hui Wan,
Mansun Chan, Ali M. Niknejad, Chenming Hu

Department of Electric Engineering and Computer Sciences, University of California at Berkeley
CA, 94720, janexi@eecs.berkeley.edu

ABSTRACT

This paper describes the next generation BSIM model for aggressively scaled CMOS technology. New features in the model include more accurate non-charge-sheet based physics, completely continuous current and derivatives, and extendibility to non-traditional CMOS based devices including SOI and double-gate MOSFETs.

Keywords: MOSFETs, compact modeling, surface-potential-plus model, small dimensional effects.

1 INTRODUCTION

Device models play a very important role in the advancement of CMOS technology and they appear ubiquitously from fabrication process development to IC design and manufacturing. The standardization procedure setup by EIA Compact Model Council (CMC)[1] helps the semiconductor industry to reduce the effort in evaluating models, and also provides directions for modeling development. Since the standardization of BSIM3V3[2], several high quality models like BSIM4 [3], SP2000 [4], HiSIM [5], EKV[6], ACM[7], USIM[8] models have emerged to meet the needs of advanced process and applications.

With the continuous scaling of CMOS technology following the ITRS roadmap, a number of the assumptions in the development of these traditional models become less valid, specifically, the charge-sheet approach ignoring the vertical carrier distribution in the inversion layer. In addition, a stronger interaction between design and modeling exists as a result of layout dependent characteristics that have been previously ignored. This is particularly true at RF and microwave frequencies where device performance such as f_{max} is a strong function of layout.

To further cope with the reduced time in the adoption of a new technology, there is need for a flexible model architecture to allow circuit simulation together with technology development, even before all physical phenomena are fully understood. To address the needs in modeling nano-CMOS, a new physical core and architecture is proposed for the next generation BSIM model. The model results in consistent, smooth and unified I-V and C-V equations that are critical in predicting distortion in analog and RF circuits. The non-charge-sheet formulation also makes the model easily extendible to non-classical CMOS devices like double-gate (DG) MOSFETs.

2 I-V MODEL FORMULATION

Accurate analytical modeling of devices in deep submicron CMOS technologies requires the physical incorporation of short-channel effects and poly-depletion, quantum effect, halo doping, retrograde doping, etc. Based on our previous work[9], SPP(Surface-Potential-Plus) is now extending to take these effects into account as well as consistent IV and CV models in quasi-2D Poisson equation solution. SPP introduces new concepts with the direct charge calculation in terms of terminal voltage, which are essential to the definition of normalized variables useful for hand calculation. By adopting a physical description of the inversion charge density and the particular structure of the model, with the derivation of continuous expressions for the MOS charges valid in all modes of operation, new deep-submicron CMOS technology effects can be simply integrated into this unified model framework, still keeping a small number of parameters. SPP core model chooses charge density rather than surface-potential as the state variable, on the other hand, maintains good computation efficiency and flexibility.

The band structure at the surface of a MOSFET is shown in Fig. 1 indicating the surface potential and the quasi-fermi potential. The relationship between charge, surface potential and quasi-fermi potential results in drift diffusion current being function of quasi-fermi potential:

$$I_{ds} = \mu_{eff} W Q_i \frac{dV_{ch}}{dy} \tag{1}$$

Following Pao-Sah's gradual channel approach and quasi-fermi potential, potential gradient equation can be derived:

$$\frac{dQ_i}{Q_i} = \frac{d\phi_s - dV_{ch}}{V_t} \tag{2}$$

And applying Gauss Law at Si-SiO_2 interface:

$$Q_i + Q_b = C_{ox}\left(V_{gb} - V_{fb} - \phi_s\right) \tag{3}$$

After eliminating the surface potential, inversion charge area density can be expressed as ($q_I = Q_I / V_t C_{ox}$, $v = V/V_t$):

$$\frac{dq_I}{q_I} + \frac{dq_I}{n_0} = \frac{dv_{GB}}{n_0} - dv_{ch} \tag{4a}$$

and

$$\ln q_I + \frac{q_I}{n_0} = \frac{v_{GB} - v_{FB}}{n_0} - \phi_B - v_{ch} \tag{4b}$$

Integrating (1) from source to drain we can get the drain current:

$$I_{ds0} = \frac{W\mu_{eff}}{L_{eff}}\left[\frac{Q_s^2 - Q_d^2}{2n_0 C_{ox}} + V_t\left(Q_s - Q_d\right)\right] \qquad (5)$$

Note that the drain current is a result of the superposition of the drift current (the Q^2 terms) and the diffusion current (the Q terms) as shown in Fig. 2.

Short channel effects are incorporated from the quasi-2D solution to Poisson equation yielding:

$$[n_0 + 2f]\left[\frac{dq_I}{q_I} + dv_{ch}\right] + dq_I = dv_{GB} + d\left(v_{DB} + v_{SB} + 2v_{bi}\right)f \qquad (6a)$$

$$\ln q_I + \frac{q_I}{n} = \frac{v_{GB} - v_{FB}}{n} + \frac{\left(v_{DB} + v_{SB} + 2v_{bi}\right)f}{n} - (\phi_B + v_{ch}) \qquad (6b)$$

Where: $n = n_0 + 2f$ and $f = \frac{1}{L}\left[1 - \exp\left(-\frac{L}{l}\right)\right]$

$$n_0 = 1 + \frac{C_d}{C_{ox}} = 1 + q_B'(\phi_s) = 1 + \frac{r}{2\sqrt{\phi_s + v_t \exp(\phi_s - 2\phi_f - v_{ch})}}$$

which can be approximated by

$$n_0 \approx 1 + \frac{r}{2\sqrt{\phi_{sa} + v_t \exp(\phi_{sa} - 2\phi_f - v_{ch})}}$$

where $\phi_{sa} = \left(\sqrt{VGB - VFB + \gamma^2/4} - \gamma/2\right)^2$

The source and drain charge can be expressed explicitly in terms of the W-Lambert equation.

Poly-depletion effects and quantum effects can be easily handled by using the n-factor and ϕ_B correction.

$$n = 1 + \frac{C_d}{C_{ox}} + \frac{N_{sub}}{N_{gate}} + \lambda_q \phi_{sa}^{-1/3} \qquad (7a)$$

$$\phi_B = \phi_{B0}\left(1 + \frac{N_{sub}}{N_{gate}}\right) + \lambda_q \phi_{s0}^{2/3} \qquad (7b)$$

The characteristics of the channel charge distribution including polysilicon depletion and quantum effect are shown in Fig. 3, indicating good agreement with 2-D and quantum numerical simulation results.

Velocity saturation, velocity overshoot and ballistic transports are handled in a unified way using the saturation charge concept with the expression:

$$Q_{dsat} = \frac{Q_s}{1 + C_{ox}E_c L/(Q_s + 2C_{ox}V_t/n)} \qquad (8)$$

The saturation drain current is given by the Ids0 expression with Q_d replaced by Q_{dsat}. With velocity overshoot based on the Price's hydrodynamic model (HD) and source-end velocity limited ballistic transport (BT), the unified drain current expression become:

$$I_{ds} = \frac{I_{ds0}}{\left[1 + \frac{Q_s - Q_d}{C_{ox}L_{eff}E_{sat}^{OV}}\right]\left[1 + \left(v_{sHD}/v_{sBT}\right)^{2\xi}\right]^{1/2\xi}} \qquad (9)$$

where v_{sHD} is the velocity from the hydrodynamic model. The model has also been extensively verified by experimental data with gate lengths down to 0.125mm and some of the results are shown in Fig. 4. The physical core also gives correct behavior for analog sensitive parameters such as gm/Id as shown in Fig. 5 with C-∞ continuity facilitating higher order harmonic analysis.

3 CHARGE AND C-V MODEL FORMULATION

The C-V equations can be directly derived from the charges calculated in the previous section resulting in a consistent I-V and C-V model with all major physical effects including poly-depletion, quantum effect, SCE, retrograde doping implemented. The C-V model is symmetric at V_{DS}=0V. The charge equation for current continuity is given by:

$$Q_i(y) = C_{ox}V_t\left(\sqrt{\left(\frac{Q_s}{C_{ox}V_t} + n\right)^2 - \frac{y}{L}\left(\frac{Q_s}{C_{ox}V_t} + n\right)^2 - \left(\frac{Q_d}{C_{ox}V_t} + n\right)} - n\right) \qquad (10)$$

The source charge and drain charge are then given by:

$$Q_s = W\int_0^L \left[1 - \frac{x}{L}\right]Q_i(x)\,dx \quad \text{and} \quad Q_d = W\int_0^L \frac{x}{L}q(x)\,dx$$

The capacitances can then calculated directly by differentiating the charges:

$$C_{XY} = \delta \cdot \frac{\partial Q_X}{\partial V_Y} = \delta \cdot \left[\frac{\partial Q_X}{\partial Q_d}\frac{\partial Q_d}{\partial V_Y} + \frac{\partial Q_X}{\partial Q_s}\frac{\partial Q_s}{\partial V_Y}\right] \qquad (11)$$

with δ =1 for X=Y and –1 otherwise. The behaviors of the terminal charges and capacitances are shown in Fig. 6, together with the result from a quantum simulator.

4 CONCLUSION

In this paper, the formulation of a modular BSIM model is described. The model exhibits smooth derivaties and is thus well suited for analog and RF applications. It also utilizes a new modular architecture with many physical effects decoupled. Advance features including layout dependent mobility, consistent non-quasi-static effects can also be incorporated. The new approach is expected to be able to accelerate the adoption of the rapid evolving CMOS technology and help to develop models together with the technology progress.

REFERENCES

[1] CMC, http://www.eigroup.org/cmc/.
[2] Y. Cheng, etal., IEEE Trans. on Electron Devices , Vol. 44, No. 2, pp. 277-287, February 1997.
[3] BSIM,http://www.device.eecs.berkeley.edu/~bsim3.
[4] G. Gildenblat, etal., pp233-240, CICC2003.
[5] M. Miura-Mattausch, etal., pp258-261, WCM2003
[6] M. Bucher, etal, pp. 670 - 673 WCM2002.
[7] C. Galup-Montoro, etal., pp. 254-257, WCM2003.
[8]H. Gummel and K.Singhal. IEEE Trans on Electron Devices, vol. 48, 1585-1593, 2001.
[9] J. He, etal, pp.262-265, WCM2003

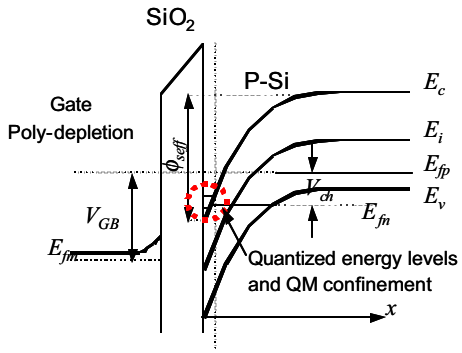

Fig. 1: The detail band diagram of a MOSFETs under strong inversion, that used to formulation equation (1)-(3)

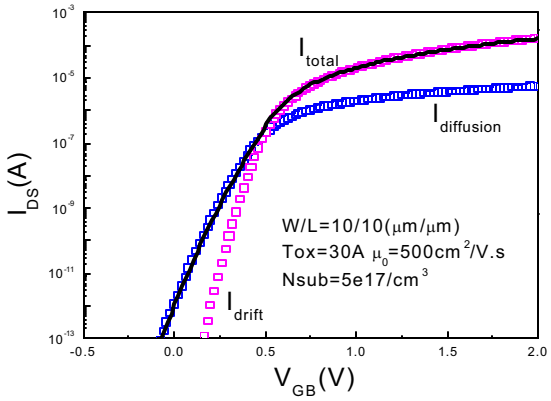

Fig. 2: Verification of drift current in strong inversion and diffusion current in subthreshold region as predicted by the new core model

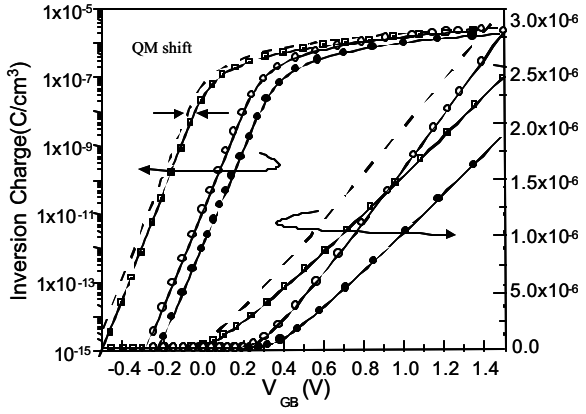

Self-consistent QME simulator
- T_{ox}=1.5nm, N_{sub}=1x10^{17}/cm^3
- T_{ox}=1.5nm, N_{sub}=1x10^{18}/cm^3
- T_{ox}=1.0nm, N_{sub}=1x10^{18}/cm^3

Model prediction with QM
Model prediction without QM

Fig. 3: Inversion charge concentration with quantum mechanical effects included as predicted by the model and comparison with self-consistent quantum mechanical simulator

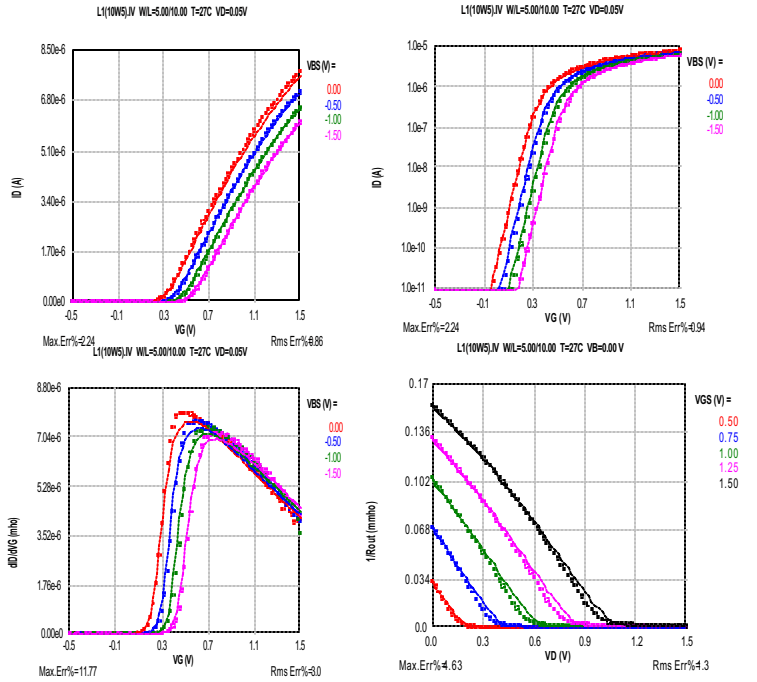

Fig. 4(a): L=10μm, W=10μm MOSFET characteristics

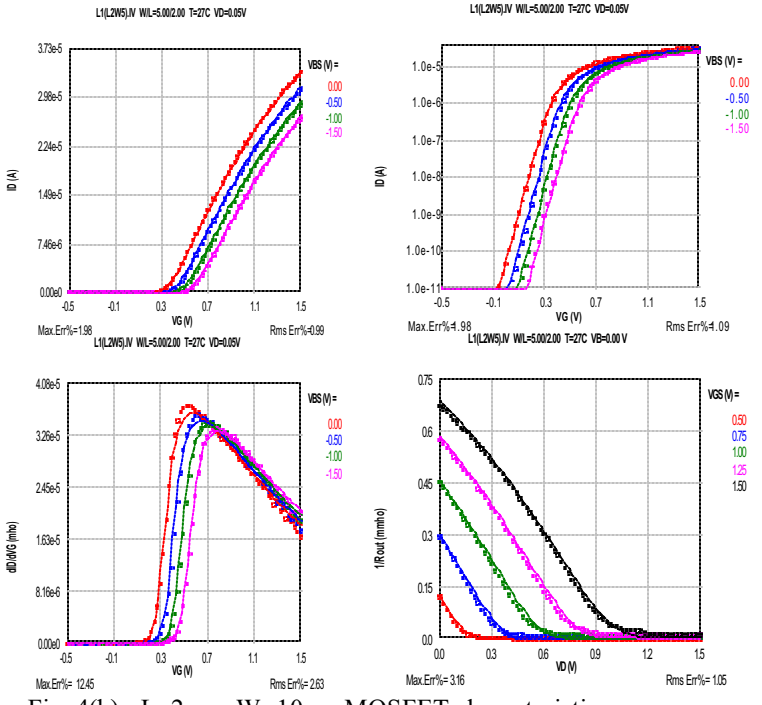

Fig. 4(b): L=2μm, W=10μm MOSFET characteristics

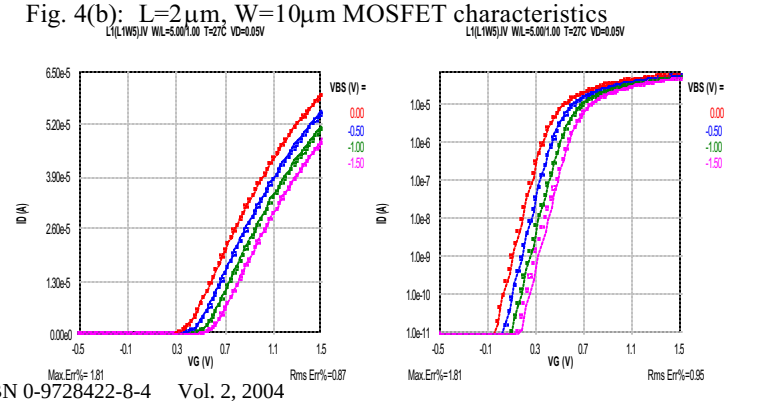

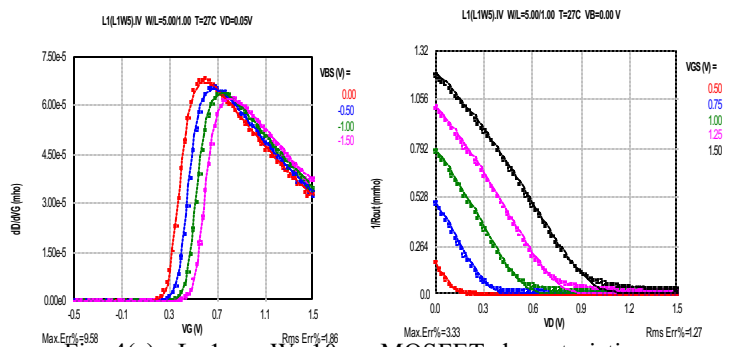

Fig. 4(c): L=1μm, W=10μm MOSFET characteristics

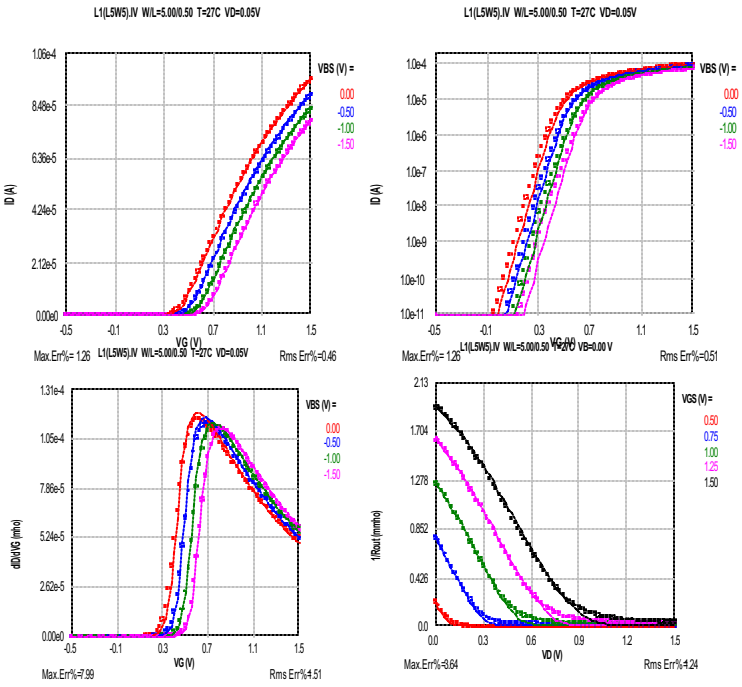

Fig. 4(d): L=0.5μm, W=10μm MOSFET characteristics

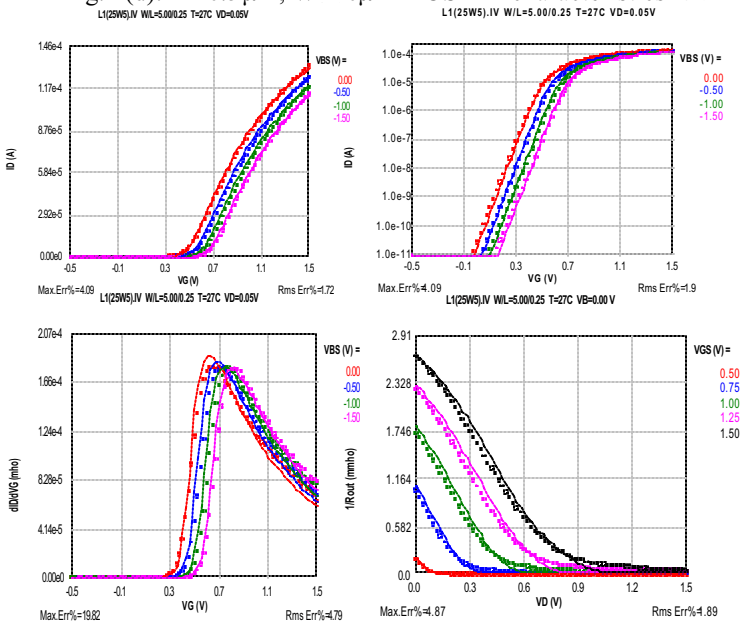

Fig.4(e): L=0.25um, W=10um MOSFET characteristics

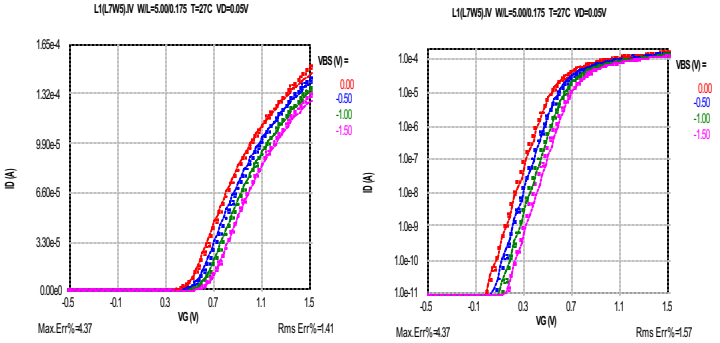

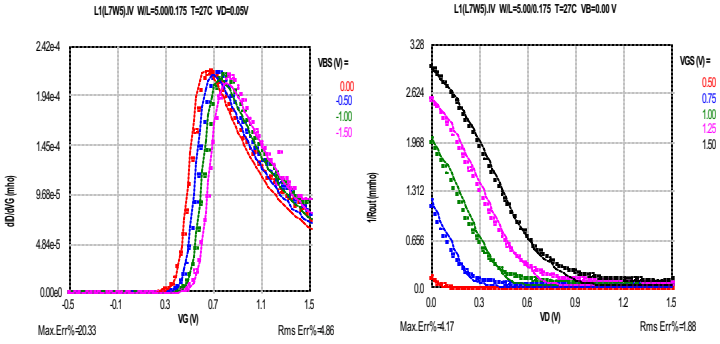

Fig. 4(e): L=0.25μm, W=10μm MOSFET characteristics

Fig.4 Comparison of I-V curves of simulation and data.

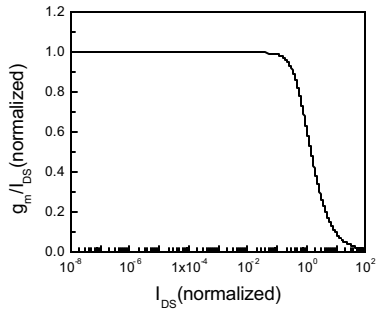

Fig. 5: The behavior of the normalized gm/IDS plot for a long channel device

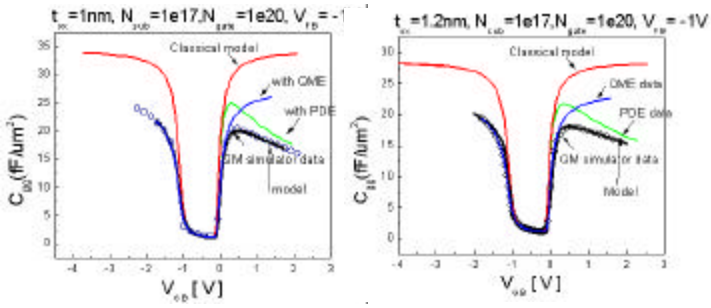

Fig.6 Comparison of Gds curves of simulation and data.